IEEE Access
Multidisciplinary | Rapid Review | Open Access Journal

Received April 9, 2022, accepted April 26, 2022, date of publication May 3, 2022, date of current version May 10, 2022.

Digital Object Identifier 10.1109/ACCESS.2022.3172300

Broadband Permittivity Characterization of a Substrate Material Using Deep Neural Network Trained With Full-Wave Simulations

LIHOUR NOV[1,2], JAE-YOUNG CHUNG[2,3], (Senior Member, IEEE), AND JAMES PARK[4]

[1]Department of Integrated IT Engineering, Seoul National University of Science and Technology, Seoul 01811, South Korea
[2]Research Center for Electrical and Technology, Seoul National University of Science and Technology, Seoul 01811, South Korea
[3]Department of Electrical and Information Engineering, Seoul National University of Science and Technology, Seoul 01811, South Korea
[4]U.S. Naval Research Laboratory, Washington, DC 20375 USA

Corresponding author: Jae-Young Chung (jychung@seoultech.ac.kr)

This work was supported by the Research Program through the Seoul National University of Science and Technology (SeoulTech).

ABSTRACT It is crucial to know the permittivity of dielectric materials used in radio frequency (RF) components and devices because their operation frequency and loss characteristics are significantly affected by the permittivity. In this study, we propose a permittivity characterization technique based on a deep neural network (DNN). The latter was trained using data obtained from full-wave electromagnetic simulation software. With the DNN trained with more than 95% testing accuracy, the measured complex transmission coefficient of the material under test (MUT) was assigned as an input to the DNN model, and the complex permittivity of the MUT was retrieved at the output. The proposed technique was validated by measuring FR-4 epoxy resin substrates of different thicknesses. The results obtained with the DNN model showed good agreement with each other, with an error of less than 1.2% for the relative permittivity value over a broad frequency range of 1 – 10 GHz. We also compared the results with those obtained from a conventional permittivity characterization technique based on analytical solutions to highlight the effectiveness of the proposed method.

INDEX TERMS Material characterization method, dielectric permittivity, relative permittivity, loss tangent, deep neural network.

I. INTRODUCTION

The permittivity indicates the amount of dipolar polarization caused by the excitation of electric fields on the dielectric. The permittivity can be expressed as a complex number [1], [2]

$$\varepsilon^* = \varepsilon_0(\varepsilon_r' - j\varepsilon_r'') = \varepsilon_0\varepsilon_r'(1 - j\tan\delta), \tag{1}$$

where $j = \sqrt{-1}$, ε_0 is the permittivity in vacuum, ε_r' is the relative permittivity, and $\tan\delta$ is the loss tangent. The latter is widely used by engineers and scientists because it indicates the amount of friction loss generated when a dielectric is exposed to high-frequency electromagnetic (EM) waves. For radio frequency (RF) or microwave engineering, ε_r' and $\tan\delta$ of a dielectric used for implementing an electric circuit, such as a substrate material of a printed circuit board (PCB), must be known because the operation frequency and loss are highly affected by these two properties. Therefore, an effective and accurate technique for measuring the permittivity of a material at high frequencies is required.

Existing permittivity measurement techniques can be categorized into three types: transmission and reflection (T/R), free-space, and resonant [3]. The resonant method is the most accurate technique, but measurement is only available around the resonant frequency of the test apparatus or its harmonic frequencies [4], [5]. The free-space method is a non-destructive technique in which a material under test (MUT) is placed in air and illuminated by broadband EM waves from a focused horn antenna pair [3], [6]. However, the required MUT size and distance from horn antennas, which are proportional to the wavelength, can be extremely large at low frequencies. For instance, at 1 GHz, a distance of

The associate editor coordinating the review of this manuscript and approving it for publication was Roberto C. Ambrosio.

6 m is required between two horns for an MUT with an area of 30 cm × 30 cm.

The T/R method [7]–[13] uses guided waves along a transmission line (Tx-line) instead of waves radiating from antennas, as in the free-space method. The MUT is inserted into or placed on a Tx-line, and then the S-parameters, such as the reflection (S_{11}) and/or transmission (S_{21}) coefficients, are measured. Subsequently, ε_r' and tanδ are retrieved from the S-parameters using the Nicolson Ross-Weir (NRW) equation [14], [15]. This closed-form equation assumes ideal transverse electromagnetic (TEM) wave propagation along the Tx-line. However, in the real world, no ideal TEM wave exists; thus, the quasi-TEM wave approximation was applied. Broadband quasi-TEM Tx-lines, such as coaxial cables or planar microstrip lines, are often used as test fixtures with moderate measurement accuracy. Nevertheless, the NRW equation cannot be used if the quasi-TEM condition is not satisfied, for example, in the case in which MUT partially fills the cross-section of a test fixture [14]. Additionally, the extraction of permittivity from the measured S-parameters information using closed-form equations assume several approximations such as dominant mode only propagation, negligible conduction loss and fringing effect, etc. This will significantly affect the extracted result accuracy.

To resolve this, a numerical technique (e.g., Newton's method [16], Monte Carlo method [17], surrogate-based method [18], and iterative comparison method [19]) can be used to retrieve the dielectric properties instead of the analytical NRW equation. However, those methods become inapplicable when applying with a large amount of data or insufficient input data will cause the model (e.g., Monte Carlo method) to perform quite poorly in the retrieving outputs. Gang *et al.* [20] has stated the limitations of inaccurately extracted dielectric permittivity results from these conventional methods based on related electromagnetic parameters using a linear or polynomial fitting. It is worth mentioning that other alternative machine learning (ML) methods such as generalized regression neural network (GRNN), support vector regression machine (SVRM), etc., have also been studied and proved to work more efficiently for a wide area of applications. However, those aforementioned algorithms are more popularly applied for modeling microwave structures (e.g., antennas) and design parameter optimizations [21], [22]. To the best knowledge of the authors, there has not been much research done so far into applying those algorithms for material characterization purposes.

From the existing neural network-based extraction methods for the complex permittivity that have been studied, there are some characterization limitations such as frequency of interests, characterizing properties, model complexity, etc. Qian *et al.* [23] provided a simple and convenient extraction method for retrieving the ε_r' using reflection coefficient data assisted by an artificial neural network (ANN) based algorithm, and proved to work effectively with less than 5% error for several organic solvents. However, the method only provides measurement results at a low frequency of 2.45 GHz. Panda *et al.* [24] had also used the ANN-based system with a coplanar waveguide (CPW) sensor to determine both the relative permittivity and loss tangent of several solid dielectric materials in a broad frequency range from 1 to 6 GHz. Additionally, these artificial intelligence (AI) based algorithms also proved to work effectively for the material characterization at sub-THz frequencies as has been illustrated in [25]. It should be emphasized that if multiple parameters are considered, e.g. the amplitude, phase, and other S-parameter data, it could significantly improve the measuring of complex dielectric permittivity results. Therefore, a deep neural network (DNN) algorithm, which is developed with several hidden layers of the single perceptron ANN model, can be one promising technique for handling such cases [26].

In this paper, we propose a novel T/R method based on a deep neural network (DNN) technique to retrieve broadband ε_r' and tanδ values from the measured S-parameters. DNN was found to be the most efficient candidate thanks to its brain-inspired neural network among several AI-supported algorithms [20]–[27]. It can efficiently provide a global minimum of an error function based on a model trained by a massive amount of data. In this work, the training data were iteratively collected by modeling the actual measurement setup in full-wave simulation software (Ansys HFSS).

The measurement fixture used in this study was a grounded coplanar waveguide (GCPW), which supports a wide bandwidth of 1 – 10 GHz. Thus, a planar MUT can be conveniently placed on the GCPW. The effectiveness of the proposed method was validated by measuring three planar printed circuit board (PCB) substrates with different thicknesses. In Section 2, the design of the GCPW fixture and overall measurement setup are described. Section 3 presents details of the permittivity retrieval process using a DNN and its parameters. Section 4 presents permittivity measurements of the FR-4 epoxy resin substrates using the proposed technique.

II. MEASUREMENT SET-UP

A planar Tx-line is widely used as a measurement fixture for RF material characterization because it allows quasi-TEM wave propagation over a broad bandwidth. The MUT can be conveniently placed on a half-opened planar structure without any exhaustive and destructive sample preparation process, which is usually required for closed structure Tx-lines such as coaxial lines or waveguides [1]. Fig. 1(a) shows the cross-section of the GCPW planar Tx-line and the electric (E) and magnetic (H) fields generated at the slots. Compared to ordinary CPW without bottom ground, GCPW confines strong E-fields at the slots owing to the metallic via truncation to the ground [19], [28]. These strong E-fields interact with the MUT at the top, whereas the electromagnetic waves propagate along the length of the Tx-line. The GCPW structure was optimized using full-wave simulation software (Ansys HFSS), and its final design parameters are listed in 1. Fig. 1(b) shows the fabricated GCPW with the MUT on top. The PCB substrate of GCPW is a 1.6 mm thick FR-4 epoxy resin. The 3.5 mm SubMiniature version A (SMA) connectors

TABLE 1. Design parameters of GCPW.

Design parameters	Value (mm)
L	90
W	41.82
t	1.89
s_gnd	19.52
g	0.45
c_t	0.035
v_s	0.2
s_t	1.6

TABLE 2. Hyper-parameter configurations of the proposed DNN model.

Parameters	Relative permittivity model	Loss tangent model
Epoch	56 000	500 000
Learning rate	0.0008	0.006
Lower-Upper constraints	3-6	0.005-0.06
Total amount of datasets	11830	11830
Training dataset ratio	0.85	0.90
Data sampling method	Random sampling	
Activation function	Scaled Exponential Linear Unit (SELU)	
Cost function	Mean Squared Error (MSE)	
Optimizer	Adam Optimizer	

TABLE 3. Performance comparison of the proposed DNN method.

Reference	Error (ε_r')	Measurement Fixture	Model Complexity
ANN Method [23] (2.45 GHz)	< 5%	OECP (Solvent Material)	Low-cost, but limited to broadband characterization capability
ANN Method [24] (1 – 6 GHz)	0.03%	CPW (CPW Material)	Built with Matlab GUI, required high local computation capacity for large amount of input data
This work, DNN Method (1 – 10 GHz)	1.20%	GCPW (Solid Material)	Fast and low-cost implementation with Google Colab platform
This work, Analytical Method	> 15%	GCPW	Fast and low-cost, but the error is too high which proved its incapability in this case of study

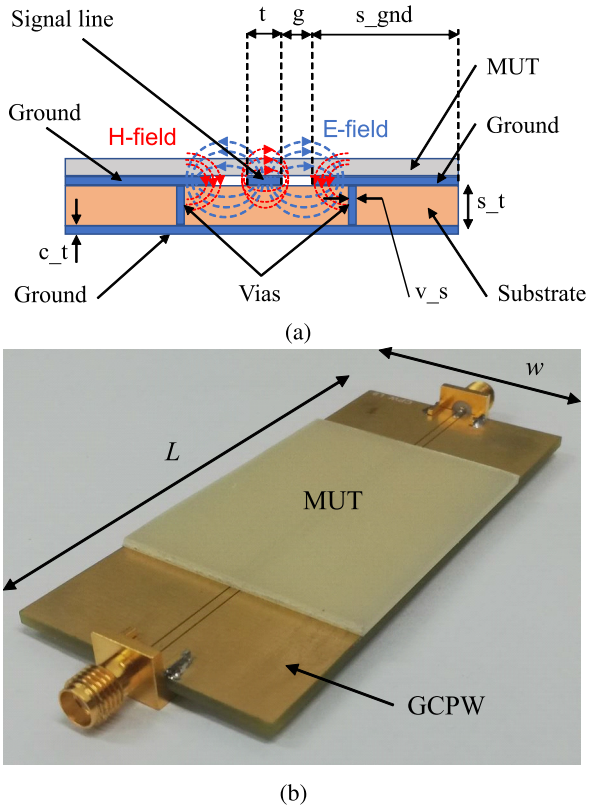

FIGURE 1. Design of the GCPW measurement fixture: (a) Cross-sectional view of the GCPW, and (b) Fabricated GCPW with MUT placed on top.

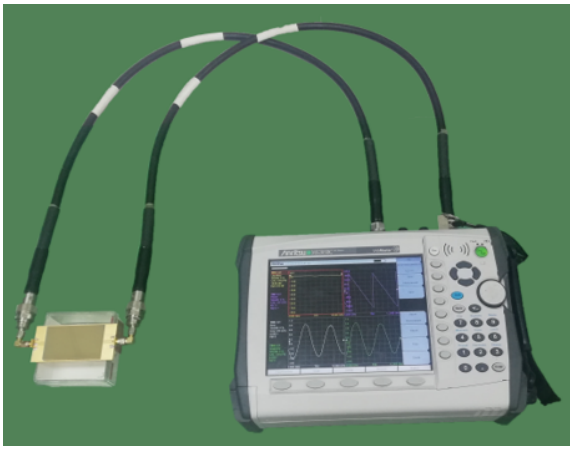

FIGURE 2. Measurement set-up: GCPW connected to a network analyzer.

were soldered at the ends of the GCPW and connected to a network analyzer (Anritsu MS2028C) for S_{21} measurements, as shown in Fig. 2. Notably, the well-known 2-port short-open-load-through (SOLT) calibration [29] was performed prior to measuring the transmission coefficient (S_{21}).

As mentioned in the introduction, one way to retrieve the dielectric properties, that is, ε_r' and tanδ, from the measured S_{21} is to use an analytical method based on closed-form equations. For GCPWs whose cross-section consists of three different materials (i.e., air, substrate, and MUT), a closed-form equation based on elliptical integration may be used [30]–[33] as long as the quasi-TEM wave propagation condition holds. However, we found non-negligible errors in the retrieved ε_r' and tanδ values when a closed-form equation was used. In contrast, the ε_r' and tanδ, that were derived from the proposed DNN method, were close to the known references. This comparison is presented and discussed in Section 4.

III. PERMITTIVITY RETRIEVAL PROCESS BASED ON DNN

The permittivity extraction based on S-parameter information requires a rigorous expression and mathematical formulation of the measurement fixture and can sometimes lead to convergence problems [24]. To alleviate this problem,

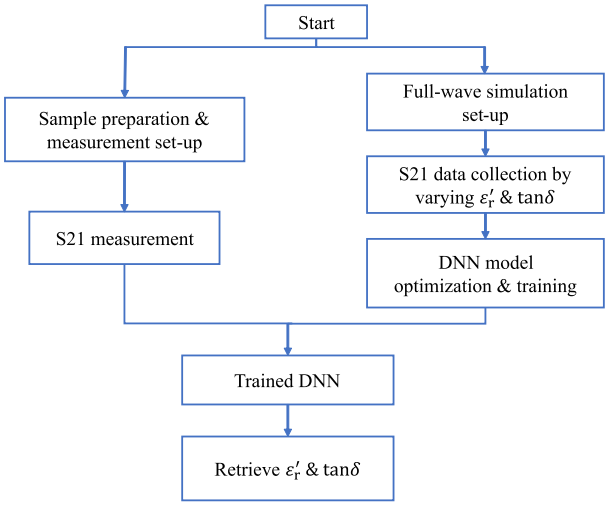

FIGURE 3. **Flow chart of the proposed permittivity characterization method.**

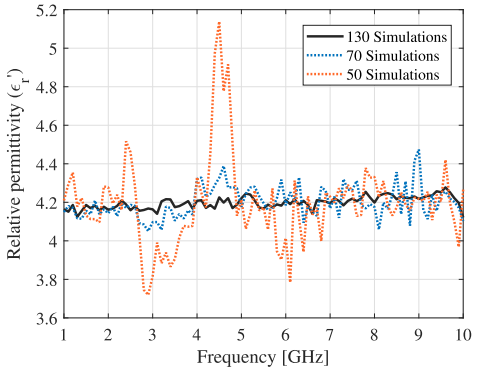

FIGURE 4. **Prediction accuracy of the ε_r' of 1.6 mm thick FR-4 regarding different amounts of input training data from 130, 70, and 50 simulations.**

many intelligent computational algorithms have been proposed and proved to work efficiently in several fields of study. More specifically, the recent AI-brained-inspired algorithm (i.e., neural network) has also played a significant role in the field of regression studies [21]. The general feedforward neural network model involved three layers including input, hidden, and output. It can be extended to a more complex model by adding several hidden layers, which is commonly called a deep neural network. The learning and training process depends significantly on the amount of sufficient input datasets and other predefined hyper-parameters (e.g., learning rate, amount of perceptron at each hidden layer, etc.) of the developed model. It should be noted that there will always be an expense of computational resources (i.e., model complexity) and achievable sufficiency model, and these should be defined appropriately based on each developed application. In our study, a fully connected pyramid-like structure has been proposed with some predefined threshold of 95% testing accuracy. Fig. 3 shows an overall flow chart of the permittivity retrieval process based on DNN. The GCPW and MUT are modeled in HFSS as in the actual S_{21} measurement. Subsequently, a number of simulated S_{21} data (approximately 130 simulations) are collected by varying ε_r' and tanδ in the simulation set-up. In the meanwhile, a macro script was implemented and used to efficiently accumulate and automatically classify the vast amount of S_{21} data. The collected S_{21} simulations are used to train the DNN algorithm. The S_{21} measurement data is inputted to the trained DNN and the ε_r' and tanδ matched to the measurement data are retrieved. The hyper-parameter configurations of the proposed DNN models for extracting ε_r' and tanδ are listed in 2. A total amount of 11830 datasets were generated considering the lower and upper constraints of ε_r' and tanδ in the frequency range of interest from 1 to 10 GHz. These datasets were split into training and testing data by a defined training ratio of 0.85 and 0.90 for ε_r' and tanδ training models, respectively.

The hyper-parameter values for the DNN model were optimized until the training accuracy is at a satisfactory level (i.e. 99% for the relative permittivity and 94% for the loss tangent). Parametric studies were performed to find the optimal model between several critical parameters including, the training accuracy, the hyper-parameters setting, the amount of input/output data, time consumption, number of hidden layers, etc. For instance, different amounts of training inputs have been studied to find the most suitable one. With an optimal number of hidden layers, we predicted the relative permittivity of a 1.6mm thick FR-4 substrate with three collected datasets from 130, 70, and 50 simulations. The predicted results were obtained as shown in Fig. 4. We observed that the choice of prediction accuracy is significantly affected by the number of datasets used. The appropriate accuracy threshold can be determined based on the given task.

Fig. 5 shows a schematic of the DNN model. The input consists of three columns: frequency, real part of S_{21}, and imaginary part of S_{21}. The outputs were ε_r' and tanδ There were 8-hidden layers between the input and the output. Each hidden layer contains a hypothesis obtained by weighting and biasing the data of the previous layer based on the weighted-sum method [27]. The mean squared error (MSE) is used as a cost function to monitor the difference between the actual values and predicted values. The cost function is updated using the Adam optimizer [34], which is inherently adapted with the backpropagation algorithm to provide suitable updated weights and bias values. A scaled exponential linear unit (SELUs) activation function is used to prevent backpropagation from the vanishing gradient problem, in which the weight is not adjusted and results in a poor training model [35]. This update ceases when the difference in the cost function is less than a defined threshold that complies with the well-trained DNN model. The DNN algorithm is written in Python and is associated with useful functions from deep learning libraries such as TensorFlow for variable declaration, NumPy for mathematical operation, and ScikitLearn for data splitting.

IV. RESULTS AND DISCUSSION

To validate the proposed technique, we measured ε_r' and tanδ of a known material. FR-4 epoxy resin substrates with

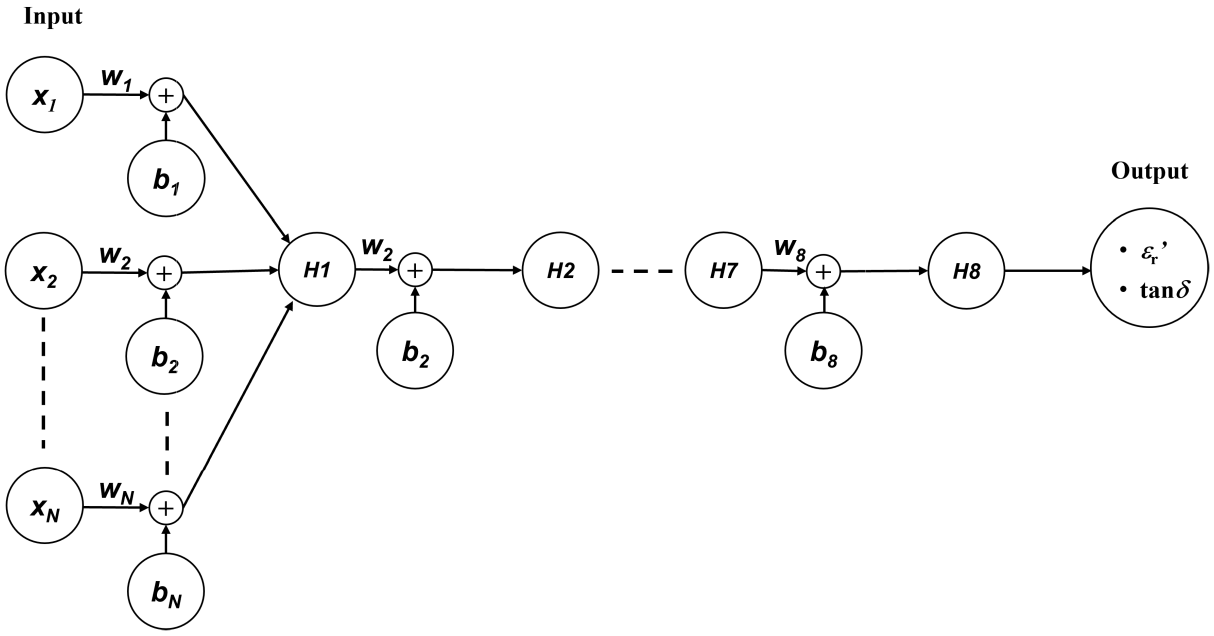

FIGURE 5. Schematic of 8-layer DNN training algorithm where *Hn* is the model hypothesis, and W_n and b_n are weighting and biasing values, respectively, at each hidden layer.

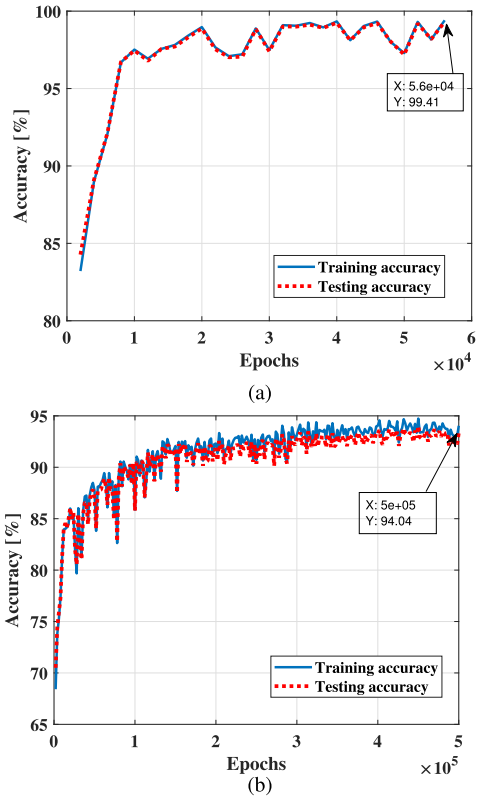

FIGURE 6. Training and testing accuracies versus number of epochs of proposed DNN model: (a) for relative permittivity prediction, and (b) for loss tangent prediction.

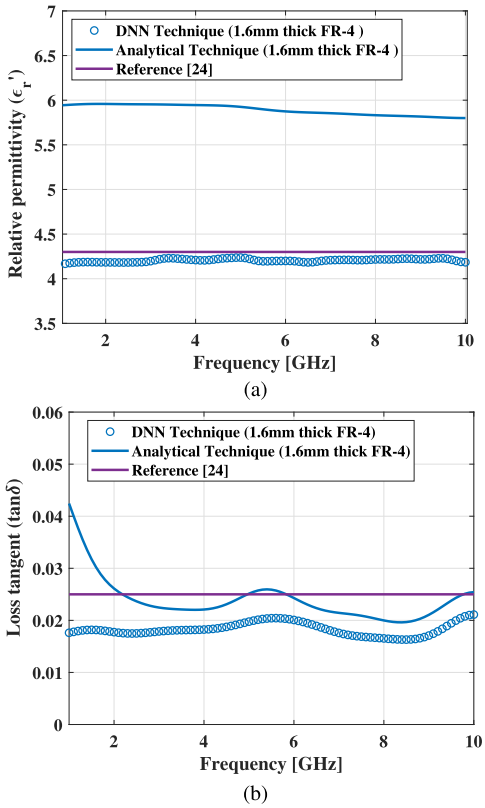

FIGURE 7. Retrieved permittivity values of 1.6 mm thick FR-4 substrate from 1 to 10 GHz by the proposed DNN method, and its comparison with the analytical method: (a) relative permittivity, and (b) loss tangent.

three different thicknesses (0.6 mm, 1.0 mm, and 1.6 mm) were prepared and placed on the GCPW one by one for S_{21} measurements. From this experiment, we expected to retrieve the same ε_r' and tanδ values from the measured S_{21}s, despite the thickness differences. It is worth noting that full-wave simulation data had to be collected from three different

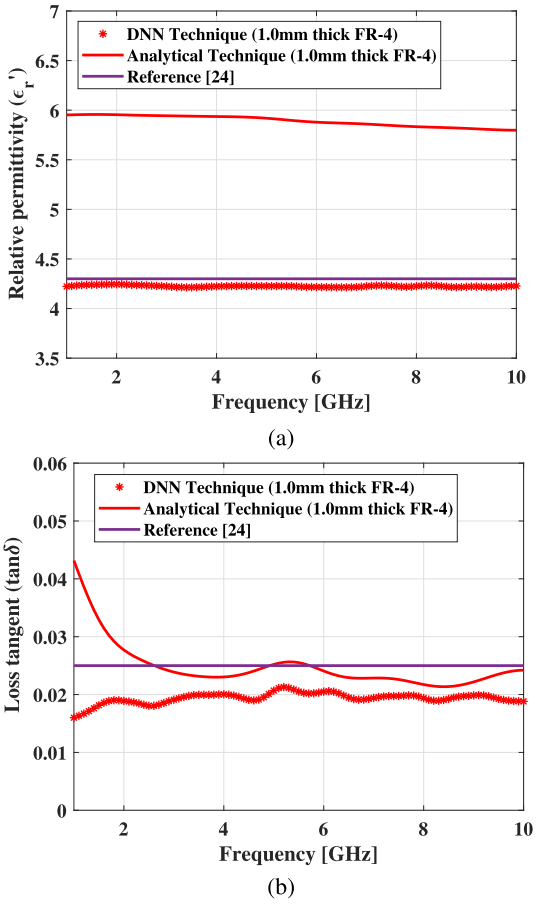

FIGURE 8. Retrieved permittivity values of 1.0 mm thick FR-4 substrate from 1 to 10 GHz by the proposed DNN method, and its comparison with the analytical method: (a) relative permittivity, and (b) loss tangent.

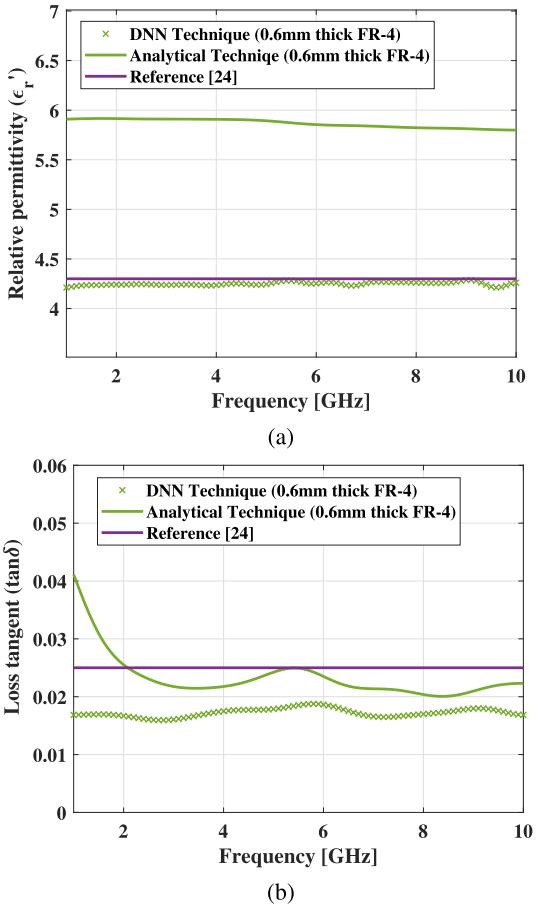

FIGURE 9. Retrieved permittivity values of 0.6 mm thick FR-4 substrate from 1 to 10 GHz by the proposed DNN method, and its comparison with the analytical method: (a) relative permittivity, and (b) loss tangent.

simulation models, while one identical DNN model for ε_r' and tanδ retrieval was used for all experiments. Thus, once the DNN model is successfully trained, it can be used in other experiments.

Fig. 6 shows the training and testing accuracies versus the number of epochs (i.e., the number of iterations of the algorithm) for the proposed DNN model. Training and testing accuracies were obtained by applying the DNN model to the training and testing data. The latter is different from the training data and is, therefore, never seen before from the DNN model viewpoint. Both Fig. 6(a) and Fig. 6(b) showed that the training and testing accuracies increased as the number of epochs increased, and they agreed well with each other. In Fig. 6(a), ε_r' prediction attains 99% accuracy with 56,000 epochs, whereas tanδ prediction, in Fig. 6(b), eventually reaches 94% accuracy with a larger number of 500,000 epochs. From this, it is expected that the retrieved ε_r' has higher accuracy than the tanδ at the end. This also corresponds to a higher error in tanδ characterization for a low-loss material when the T/R permittivity measurement method was used [36].

The trained DNN model was later used to retrieve the dielectric properties of a known FR-4 substrate with three different thicknesses. A broadband measurement of S_{21} from 1 to 10 GHz was performed for each substrate thickness of 1.6 mm, 1.0 mm, and 0.6 mm, as depicted in Fig. 2. Their ε_r' and tanδ values were subsequently retrieved, and each of the above-mentioned thickness's results were illustrated in Fig. 7, Fig. 8, and Fig. 9, respectively. As shown, they are similar to the known properties of FR-4: $\varepsilon_r' = 4.3$, and tan$\delta = 0.025$ [24] over a broad frequency range. The maximum errors from the known properties were 1.2% for ε_r' and 20% for tanδ. Furthermore, similar results for different sample thicknesses have also demonstrated the validity of the proposed technique. We also compared the ε_r' and tanδ results with those obtained from an analytical method [31], which is derived specifically based on our proposed GCPW Tx-line structure and MUT conditions (e.g., height, length). It should be noticed that the analytical extraction technique with a multilayer coplanar structure relies on measuring the transmission coefficient of the loaded material (GCPW Tx-line with MUT) and the unloaded material (standalone GCPW Tx-line), and employed the conformal mapping technique to extract the permittivity of the MUT. This technique is based on a closed-form equation, which limits the accuracy of the extracted results, and its deriving process is briefly explained in the appendix section.

A comparison of ε_r' and tanδ are shown in Fig. 7, Fig. 8, and Fig. 9 in its corresponding sub-figure (a) and (b) for the three thicknesses, respectively. As observed, the results from the analytical solution are different from the known values. The errors were 39.6% for ε_r' and 4.4% for tanδ even though the calculation was performed correctly. A large difference is observed in the extracted values for the frequency range in question, which is an unexpected result for the nondispersive FR-4 substrate. These erroneous results were due to the invalidity of maintaining the quasi-TEM conditions required for the analytical method. 3 highlights the performance comparison of the proposed method and its related counterparts for material characterization in terms of model complexity, frequency ranges, extracted parameters, and accuracy.

V. CONCLUSION

A material characterization technique based on a deep neural network (DNN) was proposed to determine the permittivity of a dielectric material, namely, the relative permittivity and loss tangent. The technique utilizes several simulation datasets that are automatically generated from full-wave electromagnetic simulator (HFSS) to be trained by our in-house developed DNN model. We performed optimization to obtain an optimum model for the relative permittivity and loss tangent, respectively. The proposed technique was validated by measuring three thicknesses of FR-4 PCB substrates, and the results agreed well with each other. Furthermore, we provided a comparison between our proposed DNN method and its related analytical method. The proposed method based on the DNN technique provides broadband characterization capability from 1 to 10 GHz with moderate accuracy. It is worth noting that the proposed technique is applicable to characterize materials other than FR-4 based on the S-parameters measured using any Tx-line structures other than GCPW as long as the full-wave simulation data for training is properly predefined and collected.

APPENDIX

The section below shows the analytical extraction technique for retrieving the permittivity of the MUT with a multi-layer coplanar structure, which is involved with S_{21} data of the loaded and unloaded MUT on the coplanar structure. Fig. 10 shows the measurement configuration of the analytical method and several involved parameters in determining the dielectric permittivity of the MUT. The derivation procedure takes into consideration the propagation constant between the loaded and unloaded MUTs [31], which is expressed in (2). The effective permittivity of the planar structure can be obtained from the complete elliptical integral of the first kind, $K(a_0)/K(a_0')$, as expressed in (3) and (4) for the unloaded and loaded MUTs, respectively.

$$\frac{S_{21}\text{Loaded}}{S_{21}\text{Unloaded}} = e^{-(\gamma_L-\gamma_U)} = e^{j\frac{2\pi}{c}fl(\sqrt{\varepsilon_{\text{eff\_U}}}-\sqrt{\varepsilon_{\text{eff\_L}}})} \tag{2}$$

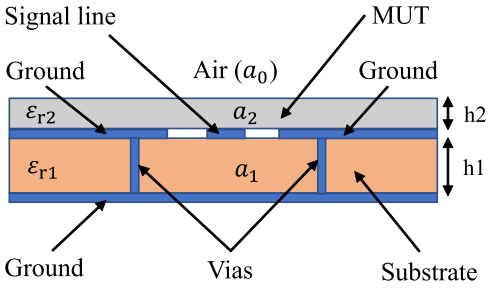

FIGURE 10. Related parameters involved in the analytical extraction technique for a multi-layer Tx-line structure, where h is the height of the substrate, ε_r is the permittivity and a is the moduli variable.

$$\varepsilon_{\text{eff\_U}} = \frac{1 + A\varepsilon_{r1}}{1 + \varepsilon_{r1}} \tag{3}$$

$$\varepsilon_{\text{eff\_L}} = \frac{2\varepsilon_0(B+(\varepsilon_{r1}-1)\frac{K(a_1)}{K(a_1')}+(\varepsilon_{r2}-1)\frac{K(a_2)}{K(a_2')})}{2\varepsilon_0 B} \tag{4}$$

where,

$$A = \frac{K(a_0)}{K(a_0')}\frac{K(a_1)}{K(a_1')}$$

$$B = \frac{K(a_0)}{K(a_0')} + \frac{K(a_1)}{K(a_1')}$$

The closed-form expression of the elliptical integral of the first type is used to determine the moduli variable "a_n" and its complementary moduli "a_n'", where their values can be obtained as in [30] and [31]. Finally, we obtained the complex permittivity of the MUT by substituting all the defined parameters in (5).

$$\varepsilon_{r2} = \{\frac{AC^2 - (A + (\varepsilon_{r1} - 1)\frac{K(a_1)}{K(a_1')})}{\frac{K(a_2)}{K(a_2')}}\} - 1 \tag{5}$$

where,

$$C = \sqrt{\varepsilon_{\text{eff\_U}}} - \frac{c\ln(\frac{S_{21}\text{Loaded}}{S_{21}\text{Unloaded}})}{2\pi fl}$$

ACKNOWLEDGEMENT

The authors thank AFOSR/AOARD for support on the Project (FA9550-18-S-0003).

REFERENCES

[1] U. C. Hasar and C. R. Westgate, "A broadband and stable method for unique complex permittivity determination of low-loss materials," *IEEE Trans. Microw. Theory Techn.*, vol. 57, no. 2, pp. 471–477, Feb. 2009, doi: 10.1109/TMTT.2008.2011242.

[2] L. F. Chen, C. K. Ong, C. P. Neo, V. V. Varadan, and V. K. Varadan, "Electromagnetic properties of materials," in *Microwave Electronics: Measurement and Materials Characterization*. Hoboken, NJ, USA: Wiley, 2004, sec. 1.3, pp. 11–28.

[3] G. Brodie, M. V. Jacob, and P. Farrell, "Techniques for measuring dielectric properties," in *Microwave and RF Technologies in Agriculture*. Poland: De Gruyter Open Poland, 2016, sec. 6 pp. 52–75.

[4] R. S. Hassan, S. I. Park, A. K. Arya, and S. Kim, "Continuous characterization of permittivity over a wide bandwidth using a cavity resonator," *J. Electromagn. Eng. Sci.*, vol. 20, no. 1, pp. 39–44, Jan. 2020.

[5] B. K. Chung, "A convenient method for complex permittivity measurement of thin materials at microwave frequencies," *J. Phys. D, Appl. Phys.*, vol. 39, no. 9, p. 1926, 2006.

[6] W.-H. Choi, W.-H. Song, and W.-J. Lee, "Broadband radar absorbing structures with a practical approach from design to fabrication," *J. Electromagn. Eng. Sci.*, vol. 20, no. 4, pp. 254–261, Oct. 2020.
[7] F. Costa, M. Borgese, M. Degiorgi, and A. Monorchio, "Electromagnetic characterisation of materials by using transmission/reflection (T/R) devices," *Electronics*, vol. 6, no. 4, p. 95, Nov. 2017.
[8] M. D. Janezic, D. F. Williams, V. Blaschke, A. Karamcheti, and C. S. Chang, "Permittivity characterization of low-k thin films from transmission-line measurements," *IEEE Trans. Microw. Theory Techn.*, vol. 51, no. 1, pp. 132–136, Jan. 2003, doi: 10.1109/TMTT.2002.806925.
[9] Z. Zhou and K. L. Melde, "A comprehensive technique to determine the broadband physically consistent material characteristics of microstrip lines," *IEEE Trans. Microw. Theory Techn.*, vol. 58, no. 1, pp. 185–194, Jan. 2010, doi: 10.1109/TMTT.2009.2036339.
[10] L. Zarral and F. Ndagijimana, "Materials characterization using a structure based on microstrip line," in *Proc. 11th Medit. Microw. Symp. (MMS)*, Sep. 2011, pp. 279–281, doi: 10.1109/MMS.2011.6068580.
[11] X. Lin and B.-C. Seet, "Dielectric characterization at millimeter waves with hybrid microstrip-line method," *IEEE Trans. Instrum. Meas.*, vol. 66, no. 11, pp. 3100–3102, Nov. 2017, doi: 10.1109/TIM.2017.2746362.
[12] J. Hu, A. Sligar, C.-H. Chang, S.-L. Lu, and R. K. Settaluri, "A grounded coplanar waveguide technique for microwave measurement of complex permittivity and permeability," *IEEE Trans. Magn.*, vol. 42, no. 7, pp. 1929–1931, Jul. 2006, doi: 10.1109/TMAG.2006.874098.
[13] S. Kim and J. Baker-Jarvis, "An approximate approach to determining the permittivity and permeability near lambda/2 resonances in transmission/reflection measurements," *Prog. Electromagn. Res. B*, vol. 58, pp. 95–109, 2014.
[14] E. J. Rothwell, J. L. Frasch, S. M. Ellison, P. Chahal, and R. O. Ouedraogo, "Analysis of the Nicolson-Ross-Weir method for characterizing the electromagnetic properties of engineered materials," *Prog. Electromagn. Res.*, vol. 157, pp. 31–47, 2016.
[15] J.-S. Kang and J.-H. Kim, "Planar offset short applicable to the calibration of a free-space material measurement system in W-band," *J. Electromagn. Eng. Sci.*, vol. 21, no. 1, pp. 51–59, Jan. 2021.
[16] T. Ozturk, A. Elhawil, M. Düğenci, İ. Ünal, and İ. Uluer, "Extracting the dielectric constant of materials using ABC-based ANNs and NRW algorithms," *J. Electromagn. Waves Appl.*, vol. 30, no. 13, pp. 1785–1799, Sep. 2016.
[17] G. Jarry, S. A. Graham, D. J. Moseley, D. J. Jaffray, J. H. Siewerdsen, and F. Verhaegen, "Characterization of scattered radiation in kV CBCT images using Monte Carlo simulations," *Med. Phys.*, vol. 33, no. 11, pp. 4320–4329, Oct. 2006.
[18] P. M. Nguyen and J.-Y. Chung, "Material properties characterization based on measurements of reflection coefficient and bandwidth," *J. Electromagn. Eng. Sci.*, vol. 14, no. 4, pp. 382–386, Dec. 2014.
[19] L. Nov and J.-Y. Chung, "Dielectric property characterisation of thin films based on iterative comparisons of full-wave simulations and measurements," *IET Sci., Meas. Technol.*, vol. 14, no. 10, pp. 992–996, Dec. 2020.
[20] H. H. Gang, D. Wang, and Z. Wang, "A permittivity measurement method based on back propagation neural network by microwave resonator," *Prog. Electromag. Res. C*, vol. 110, pp. 27–38, 2021.
[21] J. P. Jacobs, "Accurate modeling by convolutional neural-network regression of resonant frequencies of dual-band pixelated microstrip antenna," *IEEE Antennas Wireless Propag. Lett.*, vol. 20, no. 12, pp. 2417–2421, Dec. 2021, doi: 10.1109/LAWP.2021.3113389.
[22] L. Kouhalvandi, O. Ceylan, and S. Ozoguz, "Automated deep neural learning-based optimization for high performance high power amplifier designs," *IEEE Trans. Circuits Syst. I, Reg. Papers*, vol. 67, no. 12, pp. 4420–4433, Dec. 2020, doi: 10.1109/TCSI.2020.3008947.
[23] C. Qian, H. Ka-Ma, X. Yang, M. Luo, and H. Zhu, "An artificial nerve network realization in the measurement of material permittivity," *Prog. Electromag. Res.*, vol. 116, pp. 347–361, 2011.
[24] S. Panda, N. K. Tiwari, and M. J. Akhtar, "Computationally intelligent sensor system for microwave characterization of dielectric sheets," *IEEE Sensors J.*, vol. 16, no. 20, pp. 7483–7493, Oct. 2016, doi: 10.1109/JSEN.2016.2599856.
[25] M. T. Güneşer, "Artificial intelligence solution to extract the dielectric properties of materials at sub-THz frequencies," *IET Sci., Meas. Technol.*, vol. 13, no. 4, pp. 523–528, Jun. 2019.
[26] N. Calik, M. A. Belen, P. Mahouti, and S. Koziel, "Accurate modeling of frequency selective surfaces using fully-connected regression model with automated architecture determination and parameter selection based on Bayesian optimization," *IEEE Access*, vol. 9, pp. 38396–38410, 2021, doi: 10.1109/ACCESS.2021.3063523.
[27] M. Z. Alom, T. M. Taha, C. Yakopcic, S. Westberg, P. Sidike, M. S. Nasrin, M. Hasan, B. C. Van Essen, A. A. S. Awwal, and V. K. Asari, "A state-of-the-art survey on deep learning theory and architectures," *Electron*, vol. 8, no. 3, p. 292, Mar. 2019.
[28] A. Sain and K. L. Melde, "Impact of ground via placement in grounded coplanar waveguide interconnects," *IEEE Trans. Compon., Packag., Manuf. Technol.*, vol. 6, no. 1, pp. 136–144, Jan. 2016, doi: 10.1109/TCPMT.2015.2507121.
[29] J. A. Jargon, R. B. Marks, and D. K. Rytting, "Robust SOLT and alternative calibrations for four-sampler vector network analyzers," *IEEE Trans. Microw. Theory Techn.*, vol. 47, no. 10, pp. 2008–2013, Oct. 1999, doi: 10.1109/22.795076.
[30] L. A. Bronckers and A. B. Smolders, "Broadband material characterization method using a CPW with a novel calibration technique," *IEEE Antennas Wireless Propag. Lett.*, vol. 15, pp. 1763–1766, 2016, doi: 10.1109/LAWP.2016.2535115.
[31] H. Kassem and V. Vigneras, "Non-destructive measurements of dielectric constant of thin dielectric films with metallic backing using coplanar transmission line," in *Proc. 3rd Int. Conf. Adv. Comput. Tools Eng. Appl. (ACTEA)*, Jul. 2016, pp. 58–61, doi: 10.1109/ACTEA.2016.7560112.
[32] H. Kassem, V. Vigneras, and G. Lunet, "Characterization techniques for materials' properties measurement," in *Microwave and Millimeter Wave Technologies From Photonic Bandgap Devices to Antenna and Applications*. London, U.K.: IntechOpen, 2010. [Online]. Available: https://www.intechopen.com/chapters/10346, doi: 10.5772/9055.
[33] R. N. Simons, "Conductor-backed coplanar waveguide," in *Coplanar Waveguide Circuits, Components, and Systems*. New York, NY, USA: Wiley, 2001, sec. 3, pp. 87–109.
[34] Z. Zhang, "Improved Adam optimizer for deep neural networks," in *Proc. IEEE/ACM 26th Int. Symp. Quality Service (IWQoS)*, Jun. 2018, pp. 1–2, doi: 10.1109/IWQoS.2018.8624183.
[35] Y. Zhang, K. Xing, R. Bai, D. Sun, and Z. Meng, "An enhanced convolutional neural network for bearing fault diagnosis based on time–frequency image," *Measurement*, vol. 157, Jun. 2020, Art. no. 107667.
[36] J. Baker-Jarvis, E. J. Vanzura, and W. A. Kissick, "Improved technique for determining complex permittivity with the transmission/reflection method," *IEEE Trans. Microw. Theory Techn.*, vol. 38, no. 8, pp. 1096–1103, Aug. 1990, doi: 10.1109/22.57336.

LIHOUR NOV was born in Cambodia, in 1997. He received the M.S. degree in integrated IT engineering from the Seoul National University of Science and Technology, South Korea, in 2020, where he is currently pursuing the Doctoral degree in integrated IT engineering. He is also a Research Assistant with the Electromagnetic Measurement and Application (EMMA) Laboratory, Seoul National University of Science and Technology. His current research interest includes material characterization.

JAE-YOUNG CHUNG (Senior Member, IEEE) received the B.S. degree from Yonsei University, Seoul, South Korea, in 2002, and the M.S. and Ph.D. degrees from The Ohio State University, Columbus, OH, USA, in 2007 and 2010, respectively, all in electrical engineering. From 2002 to 2004, he was a RF Engineer with Motorola, South Korea. From 2010 to 2012, he was an Antenna Engineer with Samsung Electronics. He is currently an Associate Professor with the Department of Electrical and Information Engineering, Seoul National University of Science and Technology. His research interests include electromagnetic measurement and antenna design.

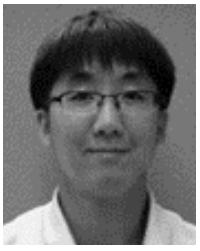

JAMES PARK received the Ph.D. degree in electrical and computer engineering from The Ohio State University, Columbus, in 2012. He is currently an Electronics Engineer with the Radar Division of the U.S. Naval Research Laboratory, Washington, DC, USA. Prior to this, he was with the Air Force Research Laboratory, Sensors Directorate, where he researched on electromagnetic scattering signatures of target and clutter. His research interests include signal/image processing problems in radar and microwave remote sensing.